Experimental Mechanics in Engineering and Biomechanics - Proceedings ICEM20
20th International Conference on Experimental Mechanics, Porto 2-7 July 2023
https://paginas.fe.up.pt/~icem20/proceedings_icem20/

PAPER REF: 19905

EXPERIMENTAL TESTING OF ACTUATOR CHAMBERS OF INTEGRATED FLUIDIC ACTUATORS FOR ADAPTIVE SLABS

Matthias J. Bosch[1(*)], Markus Nitzlader[2], Matthias Bachmann[1], Hansgeorg Binz[1], Lucio Blandini[2], Matthias Kreimeyer[1]

[1]Institute for Engineering Design and Industrial Design (IKTD), University of Stuttgart, Germany
[2]Institute for Lightweight Structures and Conceptual Design (ILEK), University of Stuttgart, Germany
[(*)]*Email:* matthias.bosch@iktd.uni-stuttgart.de

ABSTRACT

The building sector is responsible for a high CO2 footprint each year. To reduce the required resources and increase the load-bearing capacity of structural elements, designing structural elements adaptive seems to be an appropriate solution. In particular, for structural integration in adaptive slabs, conventional actuators are not suitable due to the requirements in terms of installation space and performance. Therefore, different concepts on fluidic pressure chambers for adaptive slabs are developed, tested, and compared with numerical results. The outcome of this investigation is presented in this contribution and can be used for the further development of fluidic actuators for adaptive slabs.

Keywords: experimental testing, lightweight structures, slabs, fluid actuators, adaptivity.

INTRODUCTION

Within the building sector, large amounts of resources are required for the production of cement. Combined with high process-related emissions during manufacturing, this results in a high carbon footprint (UNEP 2020). To reduce the need for cement, the mass of load-bearing civil structures, which consist to a large extent of slabs (Nitzlader et al. 2022b), must be reduced. One approach to achieve this is making the structures adaptive.

Previous investigations on linear structural elements, show the integration of actuators into the cross-section of a beam (Burghardt et al. 2022; Kelleter 2022). In a controlled manner, actuator forces are applied to counteract the deformation caused by the applied external forces. This keeps the deformation of the beam within the permissible range, compare Figure 1.

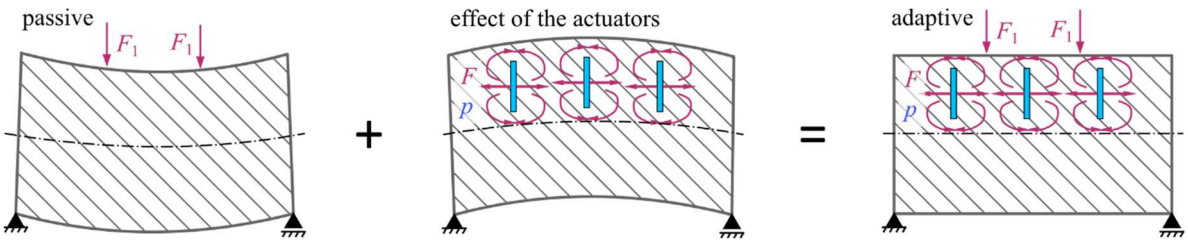

Fig. 1 – Schematic representation of an actuation concept for beams, F_1 is the force due to external load, F is the actuation force due to fluidic pressure p.

In contrast, slabs as multi-axial load-bearing elements require a more advanced actuator concept with actuators developed for this purpose, especially for acting in more than one spatial direction. As shown in the previous investigation, an actuator based on hydraulic pressure

seems to be a suitable solution due to its high energy density (Kelleter 2022). The energy conversion can be done with classical hollow-piston concepts or due to the deformation of a membrane within a pressure chamber. For the specific actuators (compare Figure 2) for slabs presented in (Nitzlader et al. 2022b; Bosch et al. 2022b) different concepts for pressure chambers are developed and investigated in preliminary tests. In addition, first FE simulations are performed to derive models for further investigations.

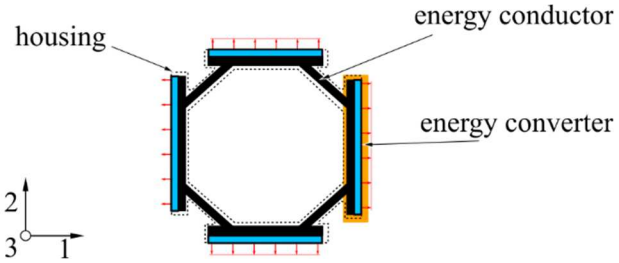

Fig. 2 – Schematic exemplary actuator with different components, the energy converter is highlighted orange.

At the beginning of this paper, an insight into the research for adaptive structures and structural elements is presented. Subsequently, the concepts for the experimental investigations, the experimental setup, and the accompanying FE models are described. Thereupon, the results are compared. Finally, a short evaluation of the concepts as well as an outlook on further investigation is given.

STATE OF RESEARCH ON ACTUATORS FOR ADAPTIVE STRUCTURES

In the future, adaptive structures offer the prospect of saving resources in the construction industry. By using sensors, actuators, and a control unit, adaptive structures can react to external loads. The first studies on this were conducted several decades ago (Soong and Manolis 1987). More recently, research on adaptive buildings and structures has been carried out at the University of Stuttgart as part of the Collaborative Research Center SFB 1244 (Sobek et al. 2021). The demonstrator high-rise building D1244 of the research center (Blandini et al. 2022) is an example of an actuated truss structure. Other works deal specifically with the actuation of concrete columns (Steffen et al. 2022), the external actuation of a prestressed concrete beam (Schnellenbach-Held et al. 2014), and the actuation of a shell (Neuhaeuser et al. 2013) to optimize load transfer. With exception of the actuation of the concrete column, the actuation is carried out with state-of-the-art actuators that are specially adapted to the task.

Senatore el al. (Senatore et al. 2019) examine the minimization of whole-life energy in the design process of adaptive structures. Within the scope of their research, the prototype of an actuated cantilever truss (Senatore et al. 2018) and a simply supported pedestrian bridge (Reksowardojo et al. 2022) were developed. Here, standard actuators were used as well.

Actuators dedicated to the integration in concrete structural elements have been developed in the past by Kelleter and Burghardt (Burghardt et al. 2022; Kelleter 2022). The concepts for beams presented in these studies are now transferred to biaxial spanning structural elements by the authors of this contribution. For this end, various topics have already been addressed, e.g. the actuation concept developed by Nitzlader et al. (2022a; 2022b) and a description of the influence of the interface between actuation and actuator concepts by Bosch et al. (2022b). For the development of actuator concepts, actuators are divided into the three functional

components energy supplier, energy converter, and energy conductor (Bosch et al. 2022a). The combination of the effect structures of the three components results in the overall actuator concept. For the energy conductor, approaches for conception and comparison were presented by (Bosch et al. 2022a). In particular, the pressurization respectively the area of the energy converter requires further detailed consideration.

CONCEPTS FOR ACTUATOR ENERGY CONVERTERS FOR ADAPTIVE SLABS

The excerpt of actuator requirements given in Table 1 can be derived from the intended actuation concept for an adaptive slab. The values given are based on the actuation concept from Nitzlader et al. (2022b).

Table 1 – Excerpt of requirement on actuators for adaptive slabs in the scope of Nitzlader et. al (2022b).

Description	Symbol	Quantity	Unit
Max. Stroke in concrete related to force and spatial extension	s / (F / l)	0,0000148	mm^2 / N
Max. Actuating force per spatial direction related to the spatial extension of the actuator	F / l	350	N / mm
Serviceability	-	Not possible	-
Leakage	-	No leakage	-

For the case study presented in (Nitzlader et al. 2022b) with a slab size of 2 m x 2 m and the aspired actuation concept, an installation height for the actuator of about 45 - 50 mm can be assumed as well as an outer edge dimension of the actuators of 130 mm x 130 mm. Depending on the flexibility and the transmission ratio of the energy conductor, the stroke provided by the energy converter must be increased. For the following investigation, a necessary stroke of 0.05 mm is assumed for an actuator with an outer edge length of 300 mm x 300 mm and a height of 50 mm. The ratio of generated force to applied force is equal to one. If a higher stroke is achievable, the energy conductor may be designed more flexible. This allows weight and material savings in the actuator structure. The necessary stroke can roughly be calculated as follows:

$$s_{\text{tot}} = (\delta_{\text{concrete}} + \delta_{\text{structure}}) \cdot F \cdot i \tag{1}$$

with: δ_{concrete}: Yield of the concrete
$\delta_{\text{structure}}$: Yield of the actuator structure
F: Applied force
i: Transmission of the actuator energy conductor

For the calculation, the flexibility of the actuator material, its cross-sectional area and length, as well as the flexibility of the concrete must be known.

Based on the given requirements a hydraulic direct drive is used due to its high energy density (compare Figure 3). Furthermore, contamination of the concrete structure with hydraulic fluid must be avoided to allow possible recycling at a later stage. Following this, a system without dynamic sealing is preferred for the hydraulic energy converter to reduce leakage as far as possible. The specification of static sealing restricts the possible energy converter concepts to

membrane and membrane bellow concepts. Here the membrane concepts are considered due to the small necessary stroke and the lower complexity. For different membrane concepts variations in the connection of the membrane to the actuator base body are possible, as well as a material variation of the membrane itself. Furthermore, the membrane can have different shapes, such as a flat membrane or a grooved membrane (Witzemann GmbH 2019). This allows manipulation of the possible stroke. In this investigation, only flat membranes will be considered. These do not require additional processing steps such as deep forming or other shaping processes. The materials used for the investigation are a metal membrane made of spring steel and a membrane made of PUR D44 90° elastomer, which is highly resistant to abrasion and hydraulic oil and is commonly used for sealing. The connection is either bolted or, as a variant in the case of spring steel, welded. The screwed version of the spring steel requires an O-ring seal, while the PUR membrane itself provides the sealing effect. The O-ring can either be a classic elastomer seal or a metal seal. For the prototype tests, elastomer seals were used due to lower accuracy requirements for the manufacturing of the base body. However, metal seals are more suitable for long-term use as they have a significantly longer service life. For this reason, metal seals are also used for sealing systems in aerospace applications.

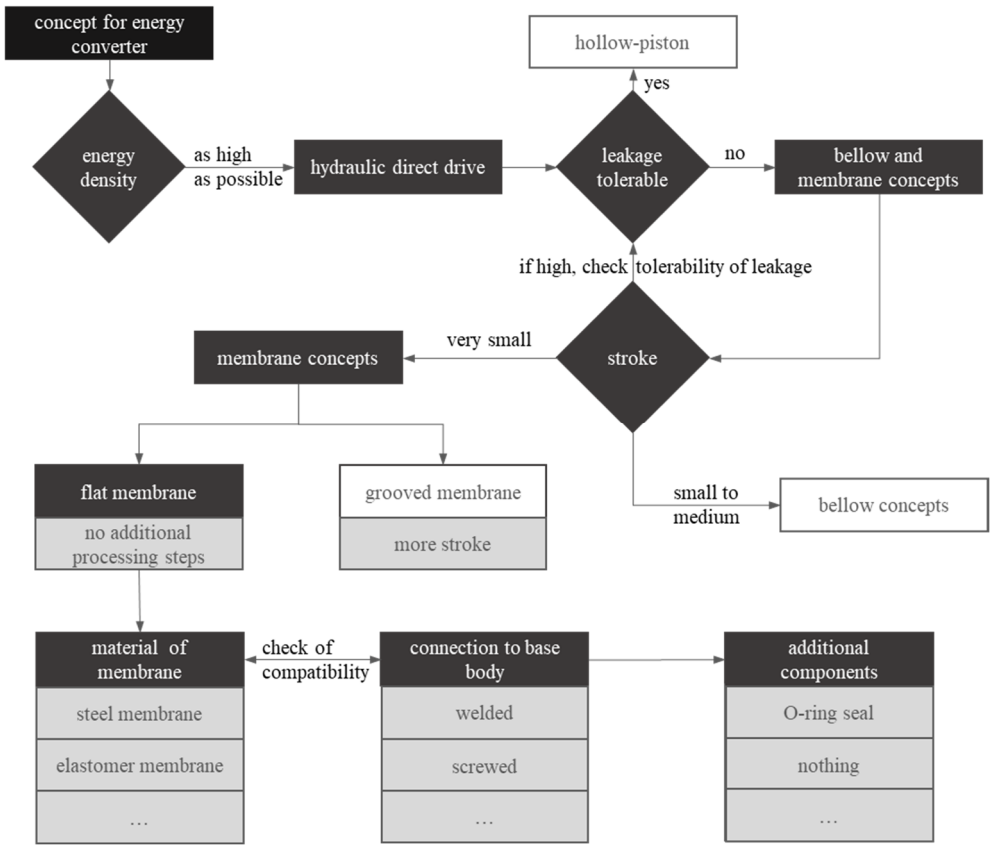

Fig. 3 – Simplified decision process for the energy converter concept.

For reasons of installation space, fastening variants other than screwing and welding seem to be not feasible. Clamping mechanisms or other designs need more installation space and are therefore not suitable for the desired field of application on thin floor slabs. It should be ensured that the connection area is as small as possible to maximize the membrane area. This leads to a reduction of the necessary hydraulic pressure.

After this consideration and determination, three concepts for the energy converter emerge when focusing on flat membrane typologies. These are schematically shown in Figure 4. In variant B, the membrane thickness is also varied between 0.5 and 1 mm. In variant C a membrane thickness of 2 mm is chosen. The realization into real test specimens is shown in Figure 5. For sealing, the elastomer in variant C was compressed by 10 % of its thickness. The pre-tensioning force of the bolt connection was set to the maximum force of an M3 8.8 screw, which delivers enough force for the necessary compression of the sealing components.

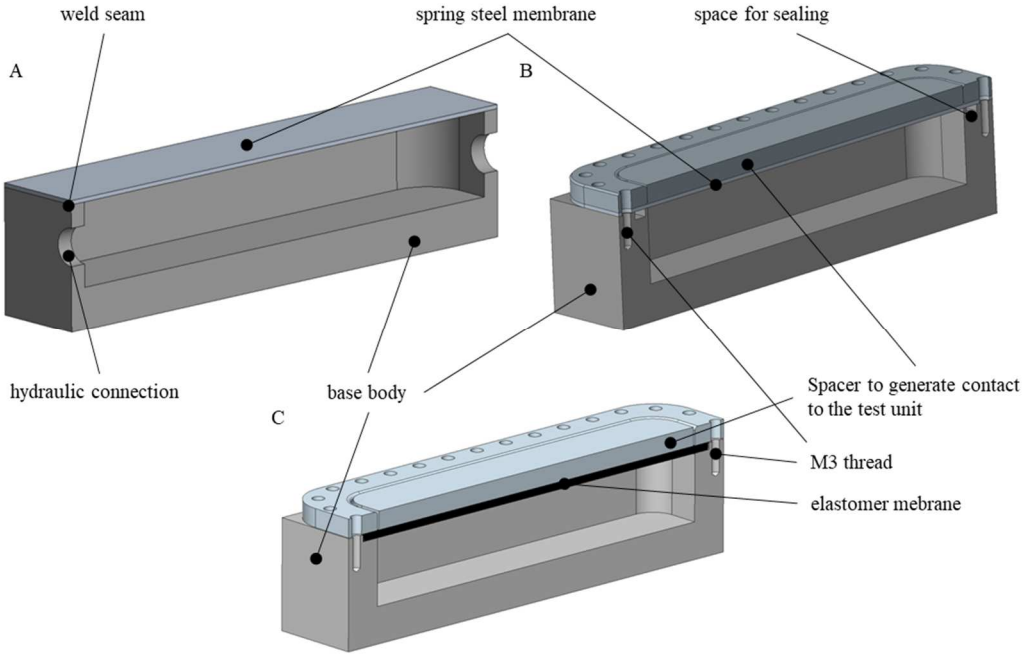

Fig. 4 – CAD model of actuator converter concepts, upper left welded spring steel (A), upper right spring steel screwed (B), lower middle elastomer membrane screwed (C).

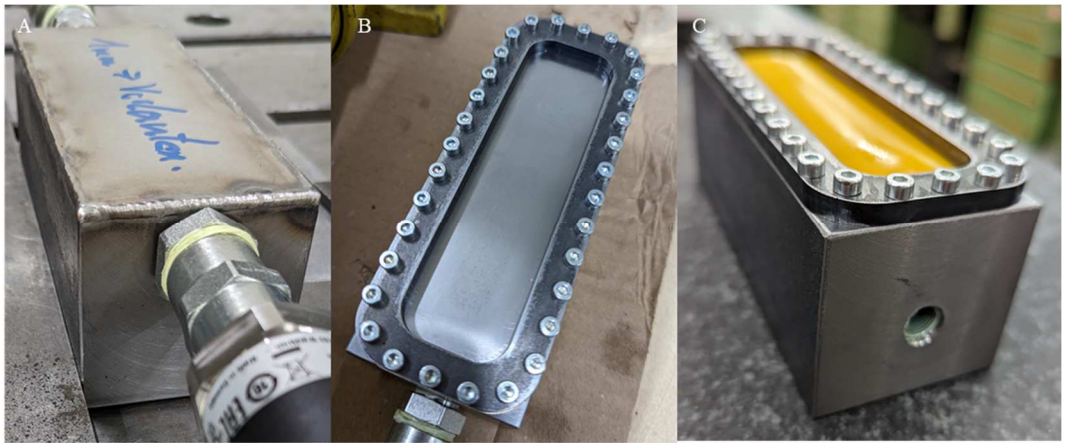

Fig. 5 – Actual prototypes for the different chamber concepts, left welded spring steel (A), middle spring steel screwed (B), right elastomer membrane screwed (C), spacers for B and C not shown.

Geometrically, the prototypes roughly correspond to the dimension of one of the four sides of an actuator for an actuation concept based on (Nitzlader et al. 2022b). The component width is 50 mm and the component length is 130 mm. If the edge area and fastening area are subtracted,

the free area of the membrane is reduced by 20 mm per spatial direction for the screwed variants and by 10 mm per spatial direction for the welded variants. From this, a force per free area (F_f^*) as well as a force related to the total installation length (F_{il}^*) are defined below:

$$F_f^* = \frac{F_m}{A_f} \tag{2}$$

$$F_{il}^* = \frac{F_m}{L_i} \tag{3}$$

Thus, on the one hand, the forces generated concerning the free area are comparable, and on the other hand, the actual generatable force in the given installation height of 50 mm can be determined.

TEST SETUP

A tension-compression testing machine was adapted to record the force generated and determine the pressure limits of the energy converters. In Figure 6 the test setup is shown. The pressure inside the chamber was built up using a hydraulic hand pump. Before testing, the pressure chamber was vented, then a pressure sensor was put on the venting pipe. By doing so, a closed hydraulic system is achieved. The pressure sensor was used to measure the pressure in the chamber, while the force was measured with a load cell inside the tension-compression testing machine.

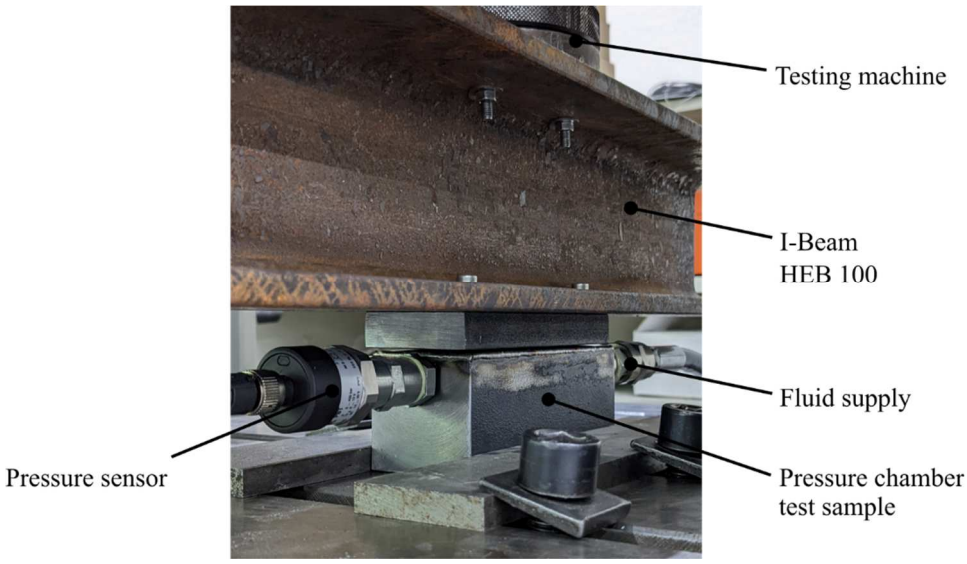

Fig. 6 – Test setup for pressure chambers.

TEST SCENARIOS

Two different test scenarios were used:

- Force controlled: application of initial force with the tension-compression testing machine, stroke for defined forces can be measured.
- Path controlled: defined initial gap between membrane and loading rig, the force for defined fixed strokes can be measured.

Table 2 – Boundary conditions for the test scenarios.

	force controlled	path controlled
variant	A	A, B, C
force range	1 000 – 5 000 N	-
stroke	-	0 – 0,05 mm
pressure limit	25 bar	200 bar
scenario number	1	2

Test scenario one was used for a pre-test. Here the force range is limited to avoid damage to the membrane when no inner pressure is applied. For variants B and C only scenario two was used. In this scenario, the force generated up to the selected pressure limit of 200 bar is determined. In addition, the forces can be displayed depending on the pressure ratio for different gap dimensions.

NUMERICAL MODEL

A simple two-dimensional numerical model was used to model the welded variant (see Figure 7). This is sufficient because the pressure chambers are significantly longer than wide. With the experimental data, the model can be tuned and validated.

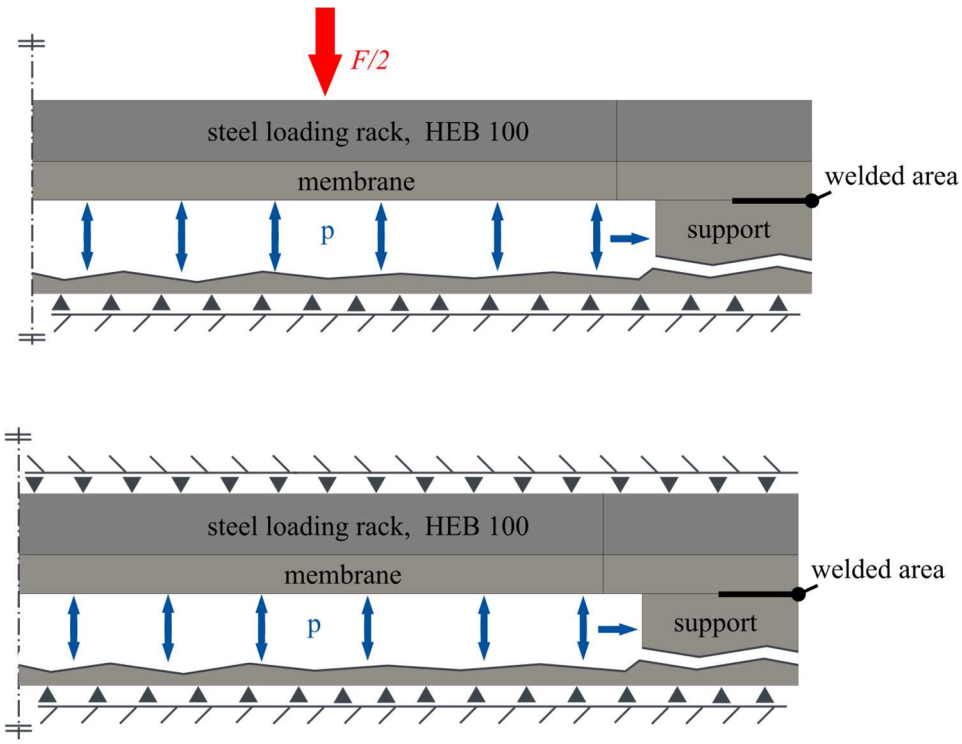

Fig. 7 – FE-model for the welded chambers (up: force controlled, down: path controlled).

A three-dimensional section was modeled for the screwed models. This allows the clamping of the membranes to be included in the simulation models. Thus, a bolted connection was modeled to obtain a pre-tensioning force in height of the maximum pre-tensioning force of an M 3 screw. In this way, all relevant effects are considered. The models are shown in Figure 8.

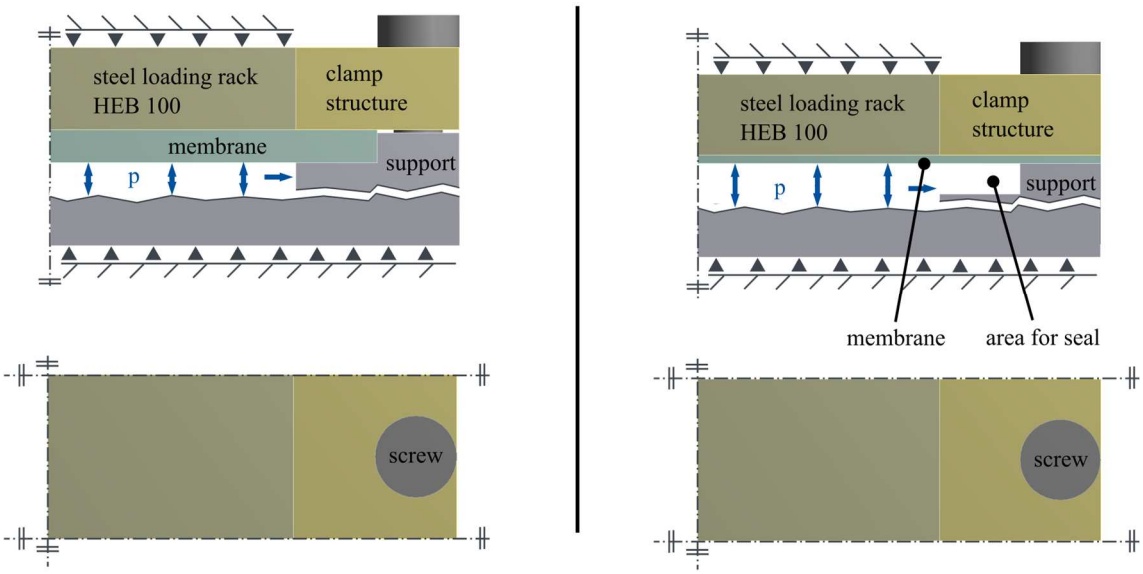

Fig. 8 – FE-model for the screwed chambers, left elastomer membrane, right spring steel membrane.

The material parameters shown in Table 3 are used for the simulations. As material models, a linear elastic model and an elastic-plastic model were compared in a pre-study. It was observed that within the scope of the study, the influence of plasticization on the magnitude of forces and deformation is negligible. Following this, a linear elastic model was chosen. For further investigation in terms of failure, an elastic-plastic model may lead to higher accuracy.

Table 3 – Material parameters for the simulation.

Description	Symbol	Unit	Spring steel, X10CrNi18-8	Structural steel, S 235	PUR-Elastomer D44 90° Shore A
Youngs's modulus	E	N/mm^2	185 000	210 000	15 (calculated)
Poisson's ratio	ν	-	0,3	0,3	0,48

RESULTS

The following results are shown for the different chamber concepts. First, the pre-study with test scenario one in comparison to the results of a tuned simulation model is shown (Figure 9). Here the experimental data and the simulation model show good consistency. As the main influence here, the length of the weld seam was detected. For good fitting data, a value as bonded contact of 50 % of the connection surface was chosen. As visible in the data, the pressure increase was stopped at a stroke of about 0.5 mm. At this point no damage to the weld seam was visible and no leakage occurred. Simulation and experiment show a linear dependence of pressure to stroke at higher pressure. It is suspected, that the initial exponential behavior is caused by the deformation of the membrane. The gap between simulation and experiment may be caused by unaccounted effects, e.g. a not perfectly tuned length of the weld seam.

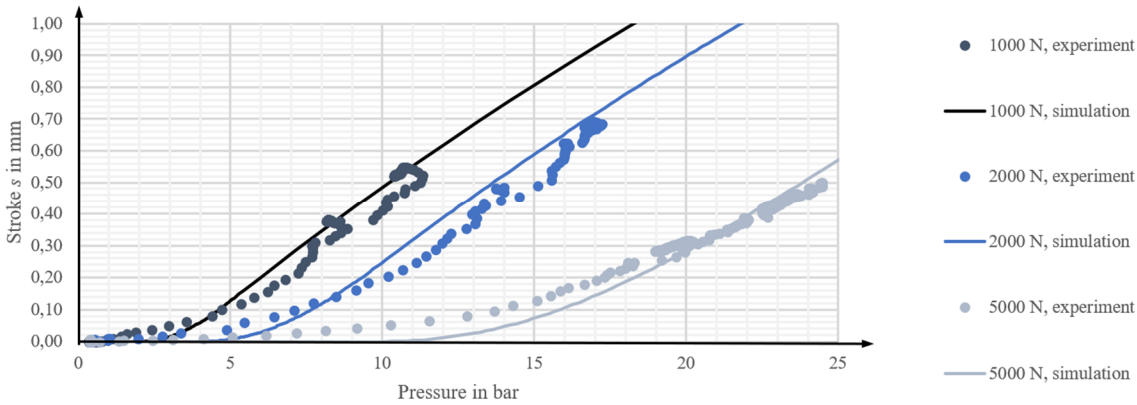

Fig. 9 – Measurement data for scenario one, variant A with experimental and simulation data.

For the second test scenario, the experimental data presented in Figure 10 are achieved. Here the experimental data normalized on the free area of the membrane is shown for the different chamber concepts and different initial gaps between the membrane and the steel loading rack. With the black line, the theoretical maximum force per free area is represented when using a classical hollow-piston hydraulic system without movement restriction. The elastomer concept leads to the highest force generation due to the most flexible material parameters, while the other concepts show a similar characteristic for the used pressure range. Additionally, it is noticeable that the curve for the elastomer stops at around 100 bar. At this point, leakage occurred and the pressure could not be increased further. In a second cycle, roughly the same pressure value was reached before leakage started again. For variant B with O-rings, small leakage occurred for a pressure above 200 bar.

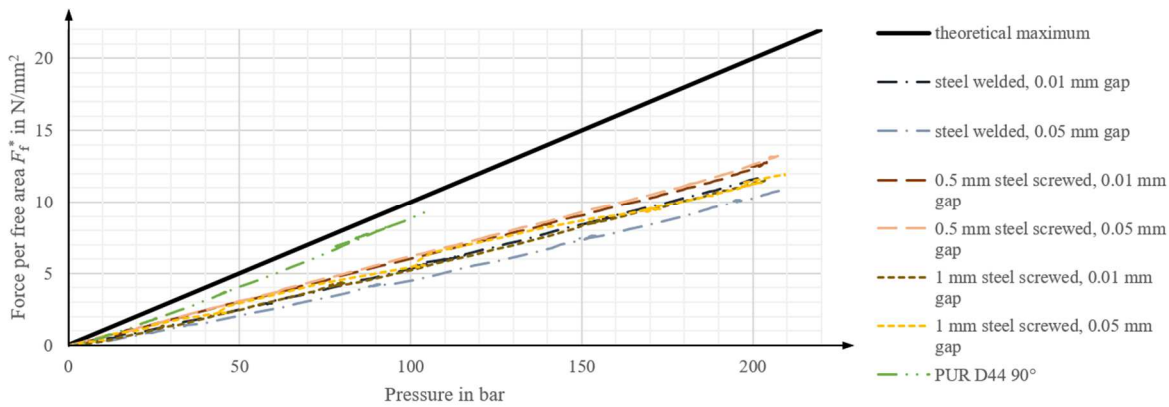

Fig. 10 – Measurement data related to free membrane area.

Looking at the force normalized to the installation length, the advantage of the welded variant is evident (compare Figure 11). This concept leads to the highest force per installation length among the others. All variants with steel membranes have in common, that they achieve the required value of 350 N/mm approximately or completely. The welded variants already reach 350 N/mm at a pressure of about 170-190 bar, depending on the initial gap. Below the point of leakage at around 100 bar, the PUR membrane reaches an even higher force per installation length than the other concepts.

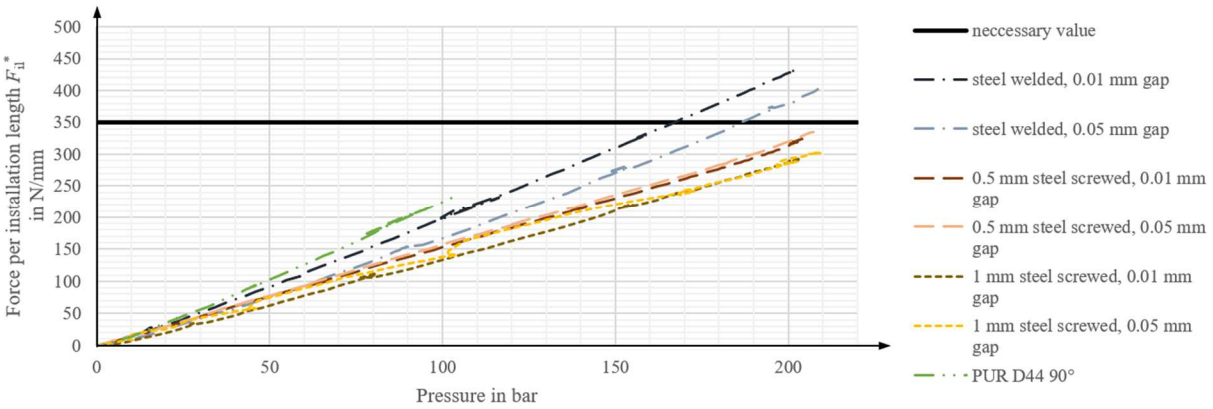

Fig. 11 – Measurement data related to installation length.

Comparing the measurement data to simulation data in Figure 12 a quite mixed picture opens up. The simulation overestimates the force per area for all models consisting of a metal membrane with a factor of 1.45. In the case of the PUR elastomer, the data fit quite well. However, the gradation between the variants is the same. Several factors could be relevant to the gap between simulation and experimental results. One factor is the reduction to a nearly two-dimensional model. Hence, the effects of constraint for the second spatial direction of the membrane are neglected. Additionally, the modeling of the contact could be further improved as well as the modeling of the deformed membrane.

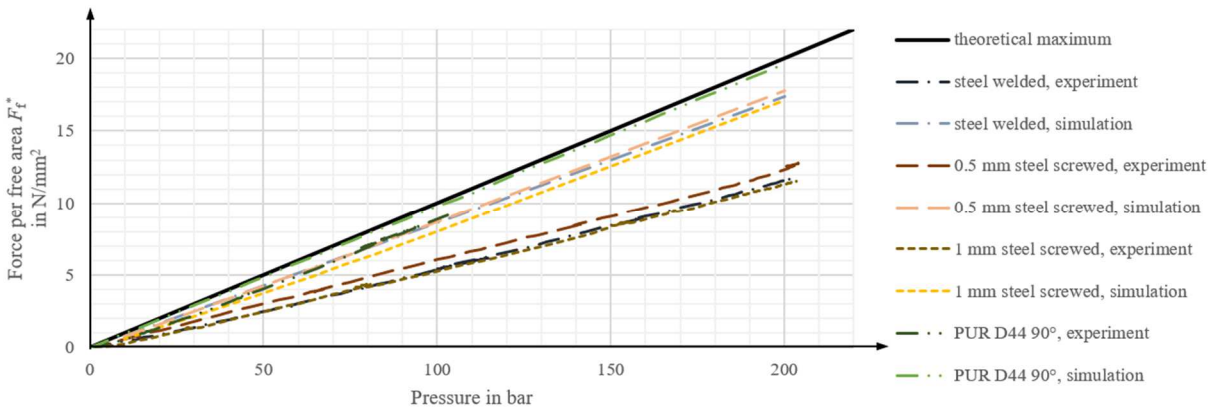

Fig. 12 – Measurement data and simulation data related to free membrane area.

CONCLUSIONS

This contribution gave an insight into the experimental investigation and the first comparison with numerical results of actuator-converter chambers. It was shown that the largest forces can be generated by the elastomer chamber in a small installation space. Here, minimal energy is required for the deformation of the membrane. A disadvantage is leakage at already low pressure compared to the other chamber variants. This could be improved with other designs, e. g. higher pre-tension or a change of the geometry of the interface between the base body and the membrane. The screwed spring steel membrane provides an acceptable result, but the force generated is lower compared to the welded version. On the other hand, critical stresses in the welded seam are avoided. For the first prototypes for integration into a slab element, the welded

variant will be pursued further due to the greater forces per installation space and higher leak tightness. From a design point of view, there is still considerable potential for the use of elastomer membranes. Furthermore, the alignment with the numerical models also needs to be further improved to lead to more satisfying results in comparison to the experimental results. Higher levels of detail in the models may lead to an improvement.

ACKNOWLEDGMENTS

This work is funded by the Deutsche Forschungsgemeinschaft (DFG, German Research Foundation) – Project-ID 279064222 – SFB 1244. The authors are grateful for the generous support.

REFERENCES

[1] Blandini L, Haase W, Weidner S, Böhm M, Burghardt T, Roth DJ et al. (2022), D1244, Design and construction of the first adaptive high-rise experimental building. In Front. Built Environ. DOI: 10.18419/opus-12333.

[2] Bosch M, Nitzlader M, Burghardt T, Bachmann M, Binz H, Blandini L, Kreimeyer M (2022a), Design of integrated fluidic actuators for muti-axial loaded structural elements. In: 8th European Congress on Computational Methods in Applied Sciences and Engineering. 8th European Congress on Computational Methods in Applied Sciences and Engineering, 2022: CIMNE.

[3] Bosch MJ, Nitzlader M, Burghardt T, Bachmann M, Binz H, Blandini L, Kreimeyer M (2022b), Effective range of integrated fluidic actuators in structural elements. In: 15th World Congress on Computational Mechanics (WCCM-XV) and 8th Asian Pacific Congress on Computational Mechanics (APCOM-VIII). 15th World Congress on Computational Mechanics (WCCM-XV) and 8th Asian Pacific Congress on Computational Mechanics (APCOM-VIII), July 31 to August 5, 2022: CIMNE.

[4] Burghardt T, Kelleter C. Bosch M, Nitzlader M, Bachmann M, Binz H et al., (2022), Investigation of a large-scale adaptive concrete beam with integrated fluidic actuators. In Civil Engineering Design 4 (1-3), pp.35-42. DOI: 10.1002/cend.202100037.

[5] Kelleter C (2022), Untersuchungen zur Manipulation des Lastabtrages biegebeanspruchter Betonbauteile durch integrierte fluidische Aktoren. Universität Stuttgart, Stuttgart. Institut für Leichtbau Entwerfen und Konstruieren.

[6] Neuhaeuser S, Weickgenannt M, Witte C, Haase W, Sawodny O, Sobek W (2013), Stuttgart smartshell - A full scale prototype of an adaptive shell structure. Dissertation. In Journal of the International Association for Shell and Spatial Structures 54 (178), pp.259-270.

[7] Nitzlader M, Bosch M, Binz H, Kreimeyer M, Blandini L (2022a), Actuation of concrete slabs under bending with integrated fluidic actuators. In: 15th World Congress on Computational Mechanics (WCCM-XV) and 8th Asian Pacific Congress on Computational Mechanics (APCOM-VIII). 15th World Congress on Computational Mechanics (WCCM-XV) and 8th Asian Pacific Congress on Computational Mechanics (APCOM-VIII), July 31 to August 5, 2022: CIMNE.

[8] Nitzlader M, Steffen S, Bosch MJ, Binz H, Kreimeyer M, Blandini L (2022b), Designing Actuation Concepts for Adaptive Slabs with Integrated Fluidic Actuators Using Influence Matrices. In CivilEng 3 (3), pp.809-830. DOI: 10.3390/civileng3030047.

[9] Reksowardojo AP, Senatore G, Srivastava A, Carroll C, Smith IFC (2022), Design and testing of a low-energy and -carbon prototype structure that adapts to loading through shape morphing. In International Journal of Solids and Structures 252, pp.111629. DOI: 10.1016/j.ijsolstr.2022.111629.

[10] Schnellenbach-Held M, Fakhouri A, Steiner D, Kühn O (2014), Adaptive Spannbetons-truktur mit lernfähigem Fuzzy-Regelungssystem. Bremen: Carl Schünemann Verlag (Forschung kompakt, 18/14).

[11] Senatore G, Duffour P, Winslow P, (2019), Synthesis of minimum energy adaptive structures. In Struct Multidisc Optim 60 (3), pp.849-877. DOI: 10.1007/s00158-019-02224-8.

[12] Senatore G, Duffour P, Winslow P, Wise C (2018), Shape control and whole-life energy assessment of an 'infinitely stiff' prototype adaptive structure. In Smart Mater. Struct. 27 (1), pp.15022. DOI: 10.1088/1361-665X/aa8cb8.

[13] Sobek W, Sawodny O, Bischoff M, Blandini L, Böhm M, Haase W et al. (2021), Adaptive Hüllen und Strukturen. In Bautechnik 98 (3), pp.208-221. DOI: 10.1002/bate.202000107.

[14] Soong TT, Manolis GD (1987), Active Structures. In J. Struct. Eng. 113 (11), pp.2290-2302. DOI: 10.1061/(asce)0733-9445(1987)113:11(2290).

[15] Steffen S, Zeller A, Böhm M, Sawodny O, Blandini L, Sobek W (2022), Actuation concepts for adaptive high-rise structures subjected to static wind loading. In Engineering Structures 267, p. 114670. DOI: 10.1016/j.engstruct.2022.114670.

[16] UNEP (2020), Status Report for Buildings and Construction: Towards a Zero-Emission, Efficient and Resilient Buildings and Construction Sector. Nairobi, Kenya.

[17] Witzemann GmbH (2019), Handbuch der Metallbälge. Pforzheim.